Nickel, copper and cobalt distribution and equilibria in Anglo Platinum furnace slags

L. Andrews[1,2] and P. C. Pistorius*[2,3]

Base metals (nickel, copper and cobalt) are recovered as part of the smelting and refining process operated by Anglo Platinum in South Africa. This study focuses on the losses of these metals to furnace slag and the effect of changing the furnace feed to include or exclude recycled oxidising converter slag. A combination of electron microbeam and Mössbauer techniques were used to characterise the base metal distribution in the slag, the variation of losses with depth in the slag bath, and the oxygen activity in the slag. Base metal dissolution into the slag is underestimated if bulk matte–slag equilibrium is assumed; predictions are closer to the observed extent of dissolution if equilibrium between entrained matte and slag is assumed, for oxygen activity controlled by the Fe^{3+}(slag)/Fe^{2+}(slag) or FeO(slag)/Fe(matte) buffers.

Keywords: Platinum, Nickel, Copper, Microanalysis, Slag, Matte

Introduction

Three smelters are operated by Anglo Platinum in the North West and Limpopo Provinces of South Africa to process platinum bearing ores. More than 80% of worldwide platinum group element reserves are found in South Africa[1] and base metals (nickel, copper and cobalt) are recovered as part of the platinum producing process. The metals are mined from the Bushveld Complex, mainly as sulphide minerals contained in the platinum ores: the Merensky reef, the Platreef and the UG-2 chromitite reef. After mining, the base metals pass through the concentrating, smelting and converting process route and are finally recovered from the nickel–copper converter matte by electrowinning at the Rustenburg Base Metals Refinery.[2]

The history and present function of the two electric furnaces at Waterval Smelter have been described before.[3,4] The furnaces are rated at 39 MVA (34 MW). Both are 8×26 m in size, and current passes between three pairs of Söderberg electrodes, situated along the length of the furnace. The interdependence between and need for careful control of slag composition, conductivity, viscosity and liquidus temperature in electric furnaces of this type have been emphasised.[5]

Blended ore concentrate is dried in flash driers, mixed with limestone flux, and then fed into the furnaces. Up until 2001, molten converter slag was returned to the furnaces, but latterly this practice has been phased out to coincide with the commissioning of two Ausmelt converters to replace the six older Peirce Smith converters. Matte from the six-in-line furnaces is tapped into ladles and granulated in water, after which it is stored before being used as converter feed. Furnace slag is tapped continuously and granulated in water. Granulated slag is then collected by rake classifiers, dewatered and stored before treatment in the slag plant, where a portion of the slag is milled and floated, and the concentrate returned to the furnaces. The nature of matte losses experienced in the slag plant has been documented.[6]

Slag and matte from two of the electric furnaces were sampled over a period of time where converter slag return to the furnaces was discontinued. This altered the Mg/Fe ratio of the slag and resulted in higher smelting temperatures. The oxygen activity in the slag also dropped, making conditions less oxidising. These factors altered the levels of base metal dissolution in, and therefore losses to, the slag, as will be described below. The results presented are from only one of the furnaces, for reasons of brevity – very little difference was observed between the two furnaces. More complete results are available elsewhere.[7]

The object of this investigation was to establish the distribution of base metals in furnace slag in order to optimise recovery. The study focused, therefore, on the losses of the base metals to the slag, as entrained sulphide and as dissolved compounds, as well as the effect of changing furnace feed and operation conditions. In addition, the viability of using equilibrium calculations to predict base metal distribution between slag and matte has been assessed, and recommendations are made to improve the outcome.

Methodology

Sampling

The furnaces were sampled once a week for four weeks over the periods of interest. Matte was sampled from the

[1]Anglo Research, PO Box 106, Crown Mines, 2025, Johannesburg, South Africa
[2]Department of Materials Science and Metallurgical Engineering, University of Pretoria, Pretoria, South Africa
[3]Department of Materials Science and Engineering, Carnegie Mellon University, 5000 Forbes Avenue, Pittsburgh, PA 15213, USA

*Corresponding author, email pistorius@cmu.edu

Published by Maney on behalf of the Institute and The AusIMM
Received 24 September 2009; accepted 26 January 2010
DOI 10.1179/037195510X12665949176418

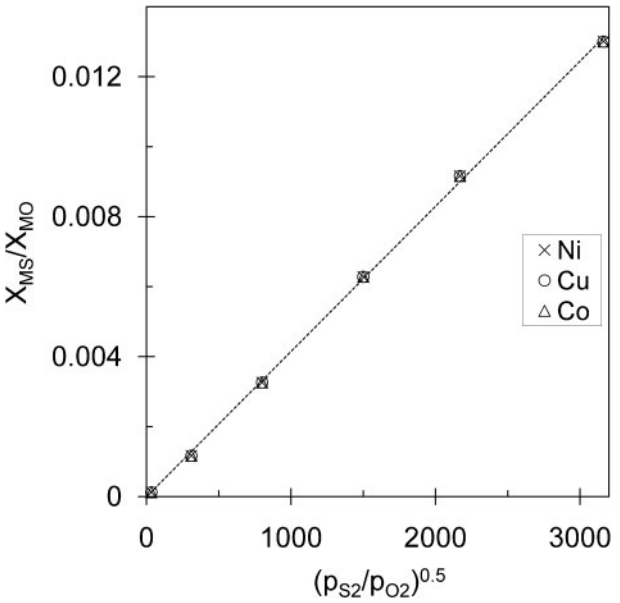

1 Calculated ratio of 'sulphidic' to 'oxidic' species of metal cations, as expected for entire range of electric furnace conditions (for temperature of 1500°C)

ladle after tapping, and tapped slag was taken as cuts across the rake classifiers after granulation in water. Samples were also taken from sounding bars dipped into the furnace, for insight into the variation of slag and entrained matte composition with depth in the furnace.

Analytical techniques

The samples were analysed in bulk using base metal fusion and inductively coupled plasma mass spectroscopy, and combustion analysis for sulphur. A combination of techniques was used to quantify the base metal distribution in furnace slag. Wavelength dispersive X-ray analysis of the slag silicate phase on the electron microprobe was combined with whole slag chemistry to provide information on the levels of dissolved metals in the slag. Entrained matte phases in the slag were analysed by energy dispersive X-ray (EDX) area analysis, and the process was automated using the Latti method, a computer controlled scanning electron microscopy (CCSEM) technique[8] which appears not to have been used before for pyrometallurgical research. The results of these analyses, run on selected samples, allowed the composition of matte droplets in the slag to be related to their apparent size. The oxygen activity in the slag was calculated from Mössbauer spectroscopy measurements of Fe^{3+}/Fe^{2+} ratios, and FactSage[9] provided predictions of base metal slag/matte partitioning. The use of the microbeam and Mössbauer techniques has previously been described in detail.[10]

Equilibrium calculations

Equilibrium calculations were performed with the Equilib module of FactSage.[9] Normalised matte compositions (Fe, Ni, Cu, Co and S) were entered, together with major elements as determined by electron microprobe analysis of the slag silicate phase. Equilibria were calculated at 1500°C, which is typical of the slag tapping temperature.

Dissolution of the base metals in the slag is predominantly in the oxidic form. An indication of the prevalence of 'oxidic' and 'sulphidic' species is given by the FactSage equilibrium calculation; the basis of this calculation was described by Pelton *et al.*,[11] with a recent update.[12] Only a brief summary is given here. Sulphur is assumed to enter the slag as sulphide ions; the sulphide capacity of the slag depends on the concentration of basic oxides (including alkali earth oxides such as MgO, CaO, and also transition metal oxides such as FeO, NiO, CoO and $CuO_{0·5}$) in the slag. The sulphide capacity of a multicomponent slag is found from the weighted average of the logarithm of the sulphide capacity, for all the basic oxides. The amount of sulphur dissolved in the slag depends on the sulphide capacity and on the partial pressures of S_2 and O_2; the ratio of the concentration of sulphidic species to oxidic species in the slag is proportional to the ratio $(p_{S_2}/p_{O_2})^{0·5}$. In the FactSage implementation of this model, it is assumed that the ratio X_{MS}/X_{MO} is the same for all oxides, where X_{MS} is the mole fraction of the 'sulphidic' species MS in the slag, and X_{MO} is the mole fraction of the 'oxidic' species MO (of the same cation M^{2+}) in the slag.

As an example of this calculation for a typical electric furnace slag, Fig. 1 shows the predicted ratio X_{MS}/X_{MO} for a slag with the composition (mass%) 21·3MgO–13·1FeO–50·5SiO_2–9·1CaO–5·4Al_2O_3, at a typical temperature of 1500°C. Amounts of 0·1% of each of NiO, CoO and Cu_2O were also added to the slag for the purpose of the calculation. Equilibrium with gas atmospheres with various ratios of $(p_{S_2}/p_{O_2})^{0·5}$ was calculated with FactSage, up to a maximum of $(p_{S_2}/p_{O_2})^{0·5} = 10^{3·5}$, which corresponds to the lowest expected oxygen activity ($\sim 10^{-7}$ atm, as discussed later), and a sulphur pressure of 1 atm. As Fig. 1 indicates, the calculated ratio of sulphidic to oxidic species is the same for all of the cations (only Ni^{2+}, Cu^{+} and Co^{2+} are shown, but it was the same for Fe^{2+}, Mg^{2+} and Ca^{2+}) – as expected from the basic assumptions of the FactSage calculation. This does not imply that the relative associations of specific cations with sulphide anions and oxygen anions in the slag are identical, but rather that this model does not distinguish this. However, it is clear that the prevalence of 'sulphidic' species is small, being less than 1·5% of the 'oxidic' species in all cases.

Results and discussion

Base metal levels and partitioning in matte and slag

Furnace matte spoon samples solidify to produce a number of sulphide and alloy phases. The most common of these are synthetic pentlandite [$(Fe,Ni,Cu)_9S_8$], troilite (FeS), bornite (Cu_5FeS_4) and minor Fe–Ni–Cu alloy. None of these phases are present in the molten matte.

When the tapped slag is granulated in water, the rapid quenching produces a product consisting almost entirely of silicate glass, in which trace amounts of nickel, copper, cobalt and sulphur are dissolved. Small entrained matte droplets are preserved as sulphide spheres. Although slag from these furnaces commonly contains minor amounts of slag spinel [$(Cr,Fe,Mg,Al)_3O_4$], this phase was present only in trace amounts in the samples examined in this study, due to relatively low chromium levels in the feed. At smelting temperatures the silicate and sulphide phases in the slag are liquid but separate – the quenched slag samples are assumed to reflect the molten nature of the

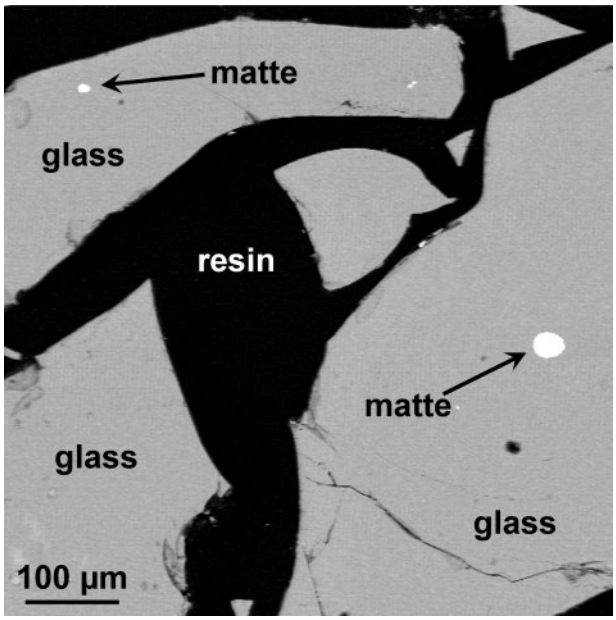

2 Typical microstructure of granulated slag: backscattered electron image of polished cross-section

slag. A typical backscattered electron image is given in Fig. 2.

Little variation is evident in furnace slag and matte compositions within the sampling periods. The results of chemical analysis of the furnace matte samples are shown in Table 1, where the earlier samples produced during converter slag return are compared to those produced after this was discontinued. Here, and throughout, these are referred to as CSR (furnace feed included converter slag return) and NCSR (no converter slag return).

The compositions of the silicate glass phases as determined with the electron microprobe are shown in Table 2. The slag also contained sodium and titanium in trace amounts. Cobalt levels were so low in the NCSR slags that this element was only analysed in two samples, using microprobe trace analysis. Oxygen is not measured using this technique, and the oxide levels are calculated by stoichiometry.

The higher Fe/Mg ratio of the CSR slag is due to the high iron content of the converter slag. Also notable are the higher dissolved base metal levels and the lower chromium content of the CSR slag. The higher levels of dissolved base metals are predominantly due to higher slag p_{O_2} – this is dealt with in more detail later in this paper. Chromium and magnesium levels were lower in

Table 1 Average compositions of tapped matte as determined by chemical analysis*, mass%

		Fe	Co	Ni	Cu	S
CSR	Average	43·99	0·52	17·87	9·44	28·19
	s.d.	1·37	0·03	0·91	0·75	0·33
NCSR	Average	41·60	0·38	17·26	11·04	29·72
	s.d.	0·34	0·02	0·78	0·58	0·46

*The standard deviations (s.d.) of the results are also shown. For comparison purposes the results have been normalised after removing contaminants from entrained slag and refractory. CSR, converter slag returned to furnace; NCSR, no converter slag return.

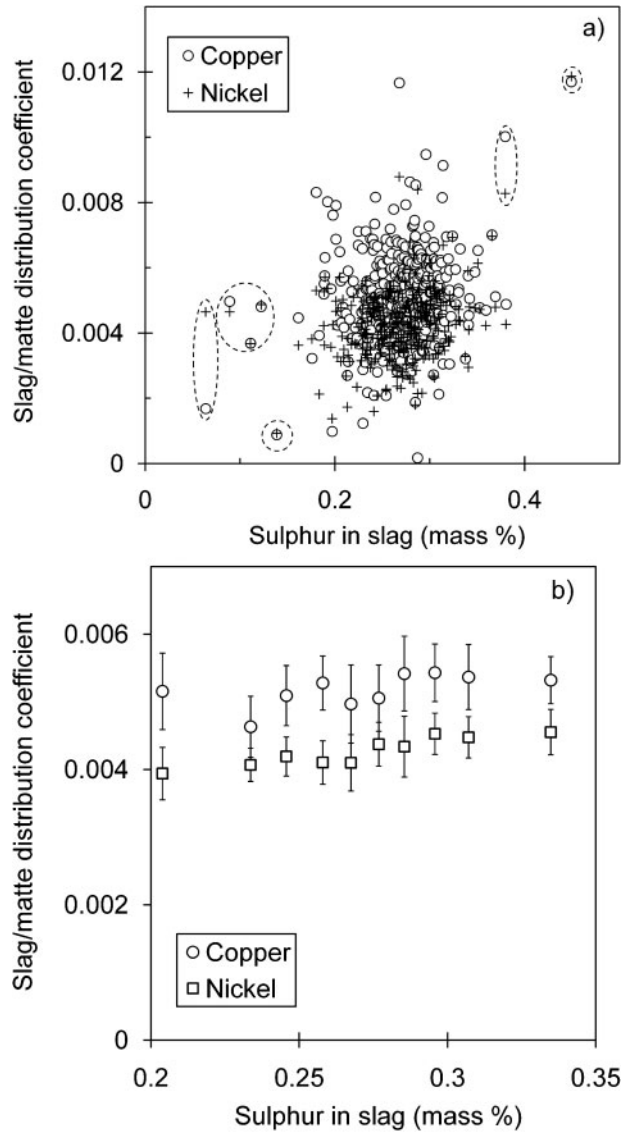

a individual analyses (all the outliers, such as those circled, originate from one sample and probably indicate some degree of microcrystallinity); *b* averages (with 95% confidence intervals, of analyses grouped by sulphur content)

3 Distribution coefficients of nickel and copper between matte and slag, as determined from slag microanalyses on all the NCSR slag samples; there is no significant change with changing sulphur content of the slag silicate phase

feeds before 2000 due to different concentrate blends and a lower UG-2 component in the feed.

The dissolved nickel and copper levels in the slag silicate are plotted against sulphur content in Fig. 3, which gives the distribution coefficients (mass percentage of the element in the slag divided by its mass percentage in the matte). Partitioning of nickel and copper between matte and slag shows no significant trend with the sulphur content of the slag, as expected since dissolution is primarily oxidic.

Entrained matte in slag

The average compositions of entrained matte phases in the slag samples are shown in Table 3. The results produced using the Latti technique are normalised, but the method was also tested against standards with

excellent results. The sulphide component of the flash drier product (furnace feed) for the later slag samples was calculated from a combination of electron microprobe and CCSEM results – feed was not sampled during the earlier campaign.

The composition of the entrained matte droplets in the tapped slag differs from that of bulk matte, being nickel rich, sulphur rich and iron depleted in comparison. The relationship between the apparent size (on polished cross-sections) and composition of the entrained matte droplets is shown in Fig. 4. Most of the droplets are under 10 μm in diameter (on polished sections), and no obvious compositional trend is evident in the 2–100 μm size range. Few droplets larger than 100 μm were present in the tapped slag, but analysis of these indicates higher Fe/Ni ratios than the smaller droplets (Fig. 4*b*); a significant trend towards bulk matte composition only occurs at larger droplet sizes, and nickel and iron appear to substitute for each other in the entrained matte. No significant trends were observed for copper or sulphur.

A typical apparent size distribution of the entrained matte droplets is shown in Fig. 5. Note that the lower cut-off size was ~2 μm, for the backscattered electron method used to detect the matte droplets. While only a few large droplets were encountered on these cross-sections, the large droplets would have a large contribution to the total mass of entrained matte. In order to assess this, it is necessary to correct the observed two-dimensional size distribution (as measured on polished planes which were presumed to intersect the sulphide droplets randomly). The droplets were assumed to be spherical (which is reasonable, given the circular appearance of the droplets in polished section). The geometry of the intersection of different polishing planes with a sphere is illustrated in Fig. 6*a*.[13] As this figure shows, a random polishing plane through a sphere gives a circular area with a radius which is smaller than that of the sphere; for example, a plane at a distance h_1 from the centre of the sphere gives a circular section with a radius of l_1, and one at a distance of (h_1+h_2) gives a radius of l_2. The effect of this is that, when apparent particle sizes are measured from a two-dimensional section, the measured particle size distribution is shifted to smaller

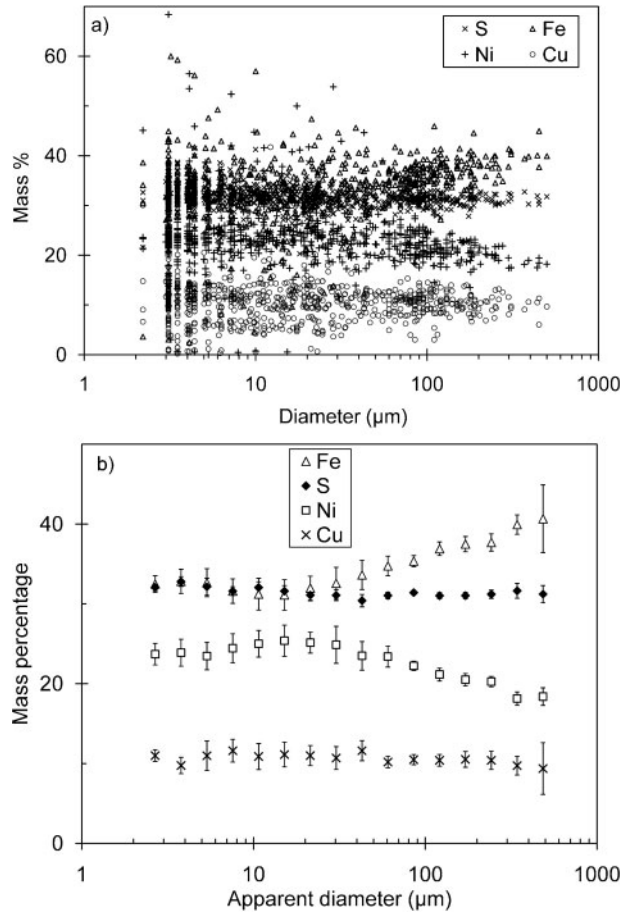

a individual analyses (the greater spread at small sizes is probably an artefact due to phase separation on cooling and the fact that the analyses were on two-dimensional sections); *b* averages (with 95% confidence intervals, of nickel, iron, copper and sulphur analyses grouped by apparent diameter of matte droplet. Only the larger droplets have a significantly higher Fe/Ni ratio)

4 Variation of entrained matte droplet composition with size (apparent diameter on polished cross-sections)

Table 2 Electron microprobe analysis results for glass phase in furnace slag samples, for furnaces operated with converter slag return (CSR) and no converter slag return (NCSR)*, mass%

Operation		MgO	Al_2O_3	SiO_2	CaO	S	Cr_2O_3	FeO	CoO	NiO	Cu_2O	Fe/Mg
CSR	1	15·86	3·73	45·66	5·89	0·42	0·87	26·54	0·070	0·152	0·095	2·1
	2	15·88	3·83	45·25	7·64	0·39	0·92	23·77	0·098	0·175	0·082	1·9
	3	14·21	4·15	42·65	13·68	0·42	0·55	22·44	0·070	0·122	0·068	2·0
	4	16·49	4·07	45·86	8·08	0·43	0·73	23·05	0·069	0·174	0·084	1·8
	G. ave	15·61	3·95	44·85	8·82	0·42	0·77	23·95	0·077	0·156	0·082	2·0
	s.d.	0·98	0·20	1·49	3·37	0·02	0·17	1·81	0·014	0·025	0·011	0·14
	Bulk	*16·40*	*3·88*	*45·95*	*9·51*	*0·47*	*0·98*	*24·12*	*0·076*	*0·191*	*0·090*	*1·9*
NCSR	1	21·09	5·11	48·04	9·80	0·28	1·42	11·95	0·014	0·088	0·065	0·73
	2	20·72	5·35	47·83	9·42	0·30	1·61	12·75	…	0·094	0·065	0·79
	3	20·40	5·17	47·59	9·61	0·24	1·30	13·17	…	0·098	0·062	0·83
	4	20·58	4·98	47·24	10·46	0·28	1·42	12·69	0·016	0·098	0·054	0·79
	G. ave	20·70	5·15	47·68	9·82	0·27	1·44	12·64	0·015	0·095	0·062	0·79
	s.d.	0·29	0·15	0·34	0·45	0·03	0·13	0·51	0·001	0·005	0·005	0·04
	Bulk	*20·90*	*5·31*	*46·78*	*10·33*	*0·30*	*1·33*	*13·12*	*0·027*	*0·175*	*0·081*	*0·81*

*Each analysis is an average of 25 (CSR) or 40 (NCSR) positions in the glass phase. Numbers 1 to 4 refer to the week of sampling. A grand average is included in the table (G. ave) as well as standard deviations (s.d.). The rows entitled with '*Bulk*' give the average bulk slag composition. Figures in italics indicate values which are closest to those measured.

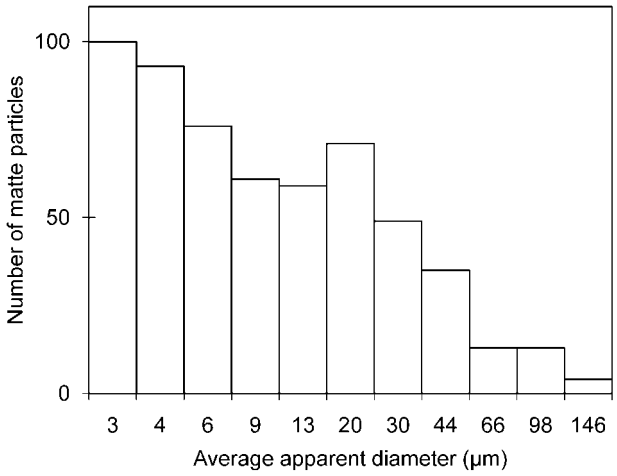

5 Apparent size distribution of matte droplets, as determined from sample cross-sections; total number of droplets was 574 (measured in sample of typical furnace slag for case of no converter slag return)

sizes than the actual three-dimensional distribution. Correcting for this requires a method to account for the larger particles which, when sectioned away from their centres, contribute to the observed number of particle sections of a given (smaller) size.

In this work, the method of Saltykov[14] was used to estimate the three-dimensional size distribution from the measured two-dimensional areas. In this method, the observed particle sections are divided into a number of size intervals (up to 12, in the published version of his method). The lower bound of each particle size interval is related to the upper bound by $d_{i+1}=(10^{-f})d_i$, with f taken to be 0·1 in the example published by Saltykov.[14] This means that the largest observed diameter is taken to be $10^{0\cdot1\times(12-1)}=12\cdot6$ times as large as the smallest observed diameter. Starting with the largest particles, the contribution of the particles, in each size interval, to observed smaller sections, is subtracted consecutively. This method is aided by the observation that, for a sphere of given diameter, the majority of random sections through the sphere have diameters which are close to the true diameter of the sphere (in Fig. 6*a*, the fraction of sections which have radii which lie between l_1 and r is equal to h_1/r, the fraction which have radii between l_1 and l_2 is equal to h_2/r, and so forth). This is illustrated by Fig. 6*b*, which gives the distribution of the

Table 3 Results, in normalised mass percentages, of averaged EDX area scans on entrained matte in two of the slag samples, for furnaces operated with converter slag return (CSR) and no converter slag return (NCSR)*

Operation	Sulphide	S	Co	Fe	Ni	Cu
CSR	Entrained matte	32·7	1·1	37·0	21·1	8·1
	Bulk matte	27·9	0·5	43·0	18·7	9·8
NCSR	Entrained matte	31·8	0·7	32·5	24·2	10·8
	Bulk matte	29·5	0·4	41·4	17·7	11·0
	Feed sulphide	37·4	0·2	38·0	14·0	10·3

*The averages were calculated on over 100 (CSR) and 500 (NCSR) phases in each sample. The normalised compositions of bulk matte and feed from same day samples are shown for comparison.

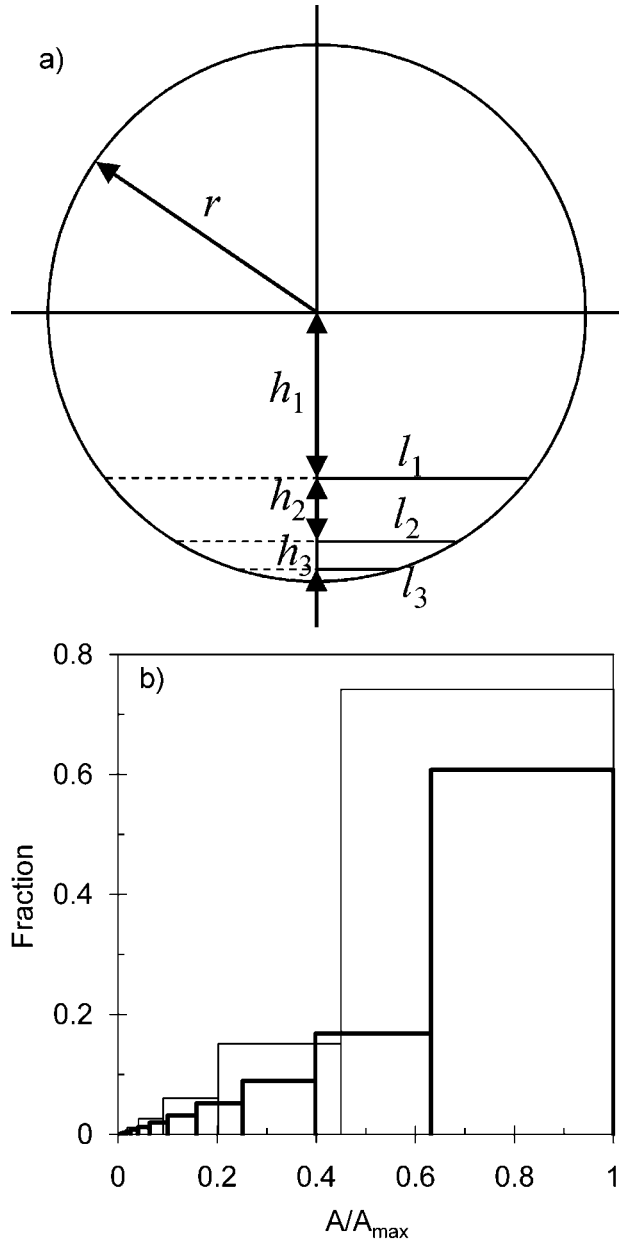

a geometry of the intersection of polishing planes with a spherical particle (radius r), with the planes at various distances (h_1, h_1+h_2, $h_1+h_2+h_3$) from the centre of the sphere, giving circular sections with radii l_1, l_2 and l_3 (adapted from Underwood);[13] *b* distribution of the areas of random sections through a sphere. Heavy line: area interval ratio of $10^{0\cdot2}$ (as used by Saltykov);[14] thin line: area interval $10^{0\cdot347}$ (as used in this work, to give a larger ratio of large to small observed sections)

6 Principle of converting from two-dimensional (cross-sectional) size distributions to three-dimensional size distributions

observed section areas. Fig. 6*b* also illustrates the area intervals which were used in this work, with a larger area ratio than that given in the paper by Saltykov.[14] This larger area ratio was necessary because the ratio of the largest to smallest observed diameters was 81 in this work (rather than 12·6 as used by Saltykov), hence requiring $f=0\cdot1735$ in this work.

The method of successively correcting for the effect of large particles on observed smaller sections is then as follows[14]

$$N_{V1} = (1/d_1)(s_1 N_{A1})$$
$$N_{V2} = (1/d_2)(s_1 N_{A2} - s_2 N_{A1})$$
$$N_{V3} = (1/d_3)(s_1 N_{A3} - s_2 N_{A2} - s_3 N_{A1})$$
$$\vdots$$
$$N_{V12} = (1/d_{12})(s_1 N_{A12} - s_2 N_{A11} - s_3 N_{A10} - s_4 N_{A9} - s_5 N_{A8} - s_6 N_{A7} - s_7 N_{A6} - s_8 N_{A5} - s_9 N_{A4} - s_{10} N_{A3} - s_{11} N_{A2} - s_{12} N_{A1})$$

In this expression, N_{Ai} is the number of particle sections with diameters between d_i and d_{i+1} which are observed on the random planes, N_{Vi} is the actual number of particles with diameter d_i in the material (that is, the required true size distribution), and s_1 to s_3 are the coefficients of the Saltykov calculation. In this work, these coefficients were recalculated for the size ratios (corresponding to f=0·1735) as required here. The original Saltykov coefficients (for f=0·1) were also recalculated, for comparison. The values for f=0·1 were found to be identical to those given in the original paper,[14] except for slight differences in s_6 to s_{12}, which coefficients appear to have been affected by truncation errors in the original paper. These values are summarised in Table 4.

The calculated true size distribution for the data of Fig. 5 is shown in Fig. 7. This confirms that the volume of entrained matte is dominated by the large droplets. Since the number of large droplets is small (Fig. 5), their volume fraction is not known accurately from microscopy. For this reason, the area density of matte droplets on cross-sections was not used to estimate the fraction of base metals lost in entrained matte. Rather, a mass balance approach based on the total slag analysis (including metal dissolved in slag and metal in entrained matte) was used, as discussed later.

Sounding bar results from both furnaces have suggested that the composition of settling matte droplets approaches that of bulk matte below tapping levels. Sounding bar samples are similar to dip samples in that interpretation of results must be made with caution. Some degree of slow cooling (crystallisation) is always evident, but neither chemical analysis nor microprobe

Table 4 Coefficients (s_i) for calculation of true size distribution by means of Saltykov method*[14]

	f=0·1		f=0·1735
i	This work	Saltykov	This work
1	1·646121	1·6461	1·348133
2	0·456123	0·4561	0·275113
3	0·11619	0·1162	0·053416
4	0·041495	0·0415	0·013822
5	0·017271	0·0173	0·004005
6	0·007795	0·0079	0·001221
7	0·003684	0·0038	0·000381
8	0·00179	0·0018	0·00012
9	0·000884	0·0010	3·81E-05
10	0·000441	0·0003	1·21E-05
11	0·000222	0·0002	3·87E-06
12	0·000112	0·0002	1·23E-06

*For f=0·1 (as in the original Saltykov paper), and f=0·1735 (as used for the sulphide droplet size distribution in this work).

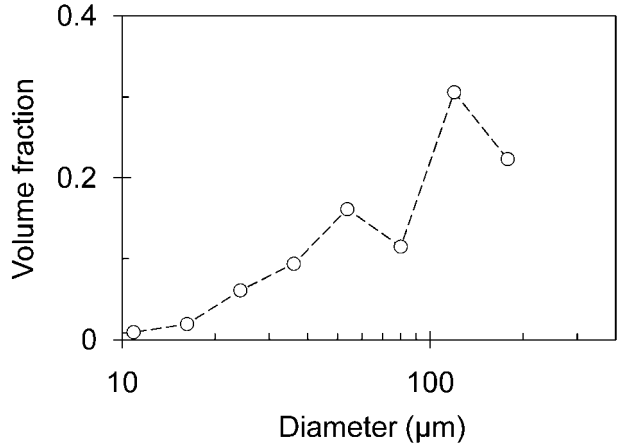

7 Calculated true size distribution for data of Fig. 5

area scans were able to detect major differences in slag silicate composition with depth in the bath. This agrees with earlier work on the furnaces.[15] Table 5 shows SEM–EDX results for entrained matte phases. In this table, depths are distances downwards from the top of the furnace; during this sampling period, the depth of the bulk matte surface was around 150–155 cm, and the lowest slag tapping level would have been 130 cm. The 145–150 cm sample of Table 5 was therefore taken from below the normal slag tapping level. Entrained matte phases in the furnace slag are scarce, so CCSEM analysis proved invaluable. The high Ni/Fe ratio compared with bulk matte and feed sulphide suggests that there is preferential entrainment of nickel rich sulphides from the concentrate, possibly because the interfacial tension of the molten sulphides varies with sulphide composition.[16]

Base metal dissolution equilibria

The reactions for oxidic dissolution of the base metals in the slag are shown below, and the equilibrium constants for these are given in Table 6. These constants were taken from the FactSage database, using liquid reference states for the matte and slag species

$$Cu + 0{\cdot}25O_2 = CuO_{0{\cdot}5} \quad K = a_{CuO_{0{\cdot}5}} / \left[a_{Cu} (p_{O_2})^{0{\cdot}25} \right]$$

$$Ni + 0{\cdot}5O_2 = NiO \quad K = a_{NiO} / \left[a_{Ni} (p_{O_2})^{0{\cdot}5} \right]$$

$$Co + 0{\cdot}5O_2 = CoO \quad K = a_{CoO} / \left[a_{Co} (p_{O_2})^{0{\cdot}5} \right]$$

Table 5 Composition of entrained matte in selected sounding bar samples taken from slag (averaged normalised mass percentage from SEM–EDX area analysis), with same day bulk matte for comparison*

Depth, cm	S	Fe	Co	Ni	Cu
78–88	29·2	35·5	0·5	27·7	7·3
95–105	30·9	38·9	0·4	20·1	9·7
145–150	31·1	41·4	0·4	18·8	8·3
Bulk matte	30·9	42·4	0·4	16·6	9·6

*Depths are distances from the furnace top, so larger depths are for samples taken lower in the slag, closer to the matte.

Table 6 Equilibrium constants for base metal dissolution*

Reaction	*A*, K	*B*
$Ni+0{\cdot}5O_2=NiO$	23 018	−8·015
$Cu+0{\cdot}25O_2=CuO_{0{\cdot}5}$	7 408·3	−2·663
$Co+0{\cdot}5O_2=CoO$	25 511	−7·384

*The equilibrium constants are given in the form $\ln K=A/T+B$, where T is the absolute temperature. Reference states are the pure liquids for the metal and oxide species.

The extent of dissolution of the metals in the slag depends on the metal activities in the matte (a_{Cu}, a_{Ni} and a_{Co}), the partial pressure of oxygen, and the activity coefficients of the metal oxides in the slag.

Prediction of the partial pressure of oxygen was based on two buffers: Fe_{matte} in equilibrium with FeO_{slag}, and equilibrium between Fe^{2+} and Fe^{3+} in the slag. The relevant reactions are

$$Fe+0{\cdot}5O_2=FeO \quad K=a_{FeO}/\left[a_{Fe}(p_{O_2})^{0{\cdot}5}\right]$$

$$FeO+0{\cdot}25O_2=FeO_{1{\cdot}5} \quad K=a_{FeO_{1{\cdot}5}}/\left[a_{FeO}(p_{O_2})^{0{\cdot}25}\right]$$

These two reactions, together with calculated activities, were used to calculate the oxygen activities. For the Fe/FeO buffer, the Fe activity in the matte was calculated using the FactSage matte model, and the FeO activity in the slag with the FactSage liquid slag model (with the measured matte and slag compositions as inputs). For the Fe^{2+}/Fe^{3+} buffer, activities of FeO and $FeO_{1{\cdot}5}$ in the slag were calculated with the FactSage liquid slag model, using the measured slag composition and measured Fe^{3+}/Fe^{2+} ratio in the slag as inputs. Ratios of Fe^{3+}/Fe^{2+} were obtained by Mössbauer spectroscopy; the average for the CSR slag samples was 0·114 and for the NCSR 0·039: when converter slag was returned to the furnaces the slags were considerably more oxidising.

The predicted partial pressure of oxygen for the two buffers is shown in Table 7; average entrained matte compositions and tapped bulk matte were used in the calculations. The activity of iron is very different in the entrained matted droplets and in the bulk (tapped) matte (because of the large difference in composition of entrained and bulk matte), resulting in different partial pressures of oxygen for the Fe/FeO buffer when presuming equilibrium between FeO in the slag, and Fe in respectively entrained and tapped matte.

Because of the differences in oxygen activities of the buffers and differences in the metal activities in the bulk and entrained matte, the calculated extents of dissolution of nickel, copper and cobalt in the slag differed and are reported in Table 8. Comparison with the actual extents of dissolution in the slag (Table 2) shows that the tapped slag is more likely to be in equilibrium with entrained matte (or perhaps with the overlying concentrate) than with bulk matte.

This conclusion is paralleled by data on temperature profiles through the slag layer.[5] Current tapping practice precludes slag tapping from within 20 cm above the matte/slag interface and from within 30 cm below the overlying concentrate; this results in slag tapping temperatures which are normally at least 100°C higher than those of matte. Entrained matte within the slag layer is hence not in thermal equilibrium with the bulk matte, indicating a lack of physical interaction between tapped slag and tapped matte. This also manifests itself in chemical non-equilibrium between tapped slag and tapped (bulk) matte.

Process optimisation

Losses of base metals to Anglo Platinum furnace slags are by oxidic dissolution in the slag, and as entrained matte. Since the slags are not treated further by pyrometallurgical reduction, losses by dissolution in slag are not recoverable. A limited amount of furnace slag is currently milled and floated in the slag plant where the coarser entrained matte particles should be recovered. However, a substantial proportion of slag is

Table 7 Matte activities and predicted partial pressure of oxygen p_{O_2} for Fe^{3+}/Fe^{2+} and Fe/FeO buffers

		Activities (liquid reference)				p_{O_2}, atm	
Operation	Matte	Fe	Ni	Cu	Co	Fe^{3+}/Fe^{2+}	Fe/FeO
CSR	Bulk	0·184	0·141	0·0452	0·0041	$9{\cdot}7\times10^{-5}$	$1{\cdot}2\times10^{-9}$
	Entrained	0·012	0·035	0·0075	0·0012	$9{\cdot}7\times10^{-5}$	$3{\cdot}1\times10^{-7}$
NCSR	Bulk	0·106	0·110	0·0344	0·0023	$6{\cdot}7\times10^{-6}$	$1{\cdot}6\times10^{-9}$
	Entrained	0·010	0·036	0·0101	0·0007	$6{\cdot}7\times10^{-6}$	$1{\cdot}8\times10^{-7}$

Table 8 Predicted dissolved base metal content for slag in equilibrium with bulk and entrained matte for buffers of Table 7*

		NiO, %		Cu_2O, %		CoO, %	
Operation	Slag/matte equilibrium	Fe^{3+}/Fe^{2+}	Fe/FeO	Fe^{3+}/Fe^{2+}	Fe/FeO	Fe^{3+}/Fe^{2+}	Fe/FeO
CSR	Bulk	8·569	0·031	0·528	0·032	4·907	0·018
	Entrained	2·114	*0·120*	*0·088*	0·021	1·385	*0·078*
NCSR	Bulk	1·164	0·018	0·177	0·022	0·586	*0·009*
	Entrained	0·378	*0·062*	*0·052*	0·021	0·176	*0·029*

*T=1500°C; a_{FeO}=0·210 (CSR) and 0·139 (NCSR) (liquid reference). Figures in italics indicate values which are closest to those measured.

Table 9 Proportion of base metal loss to slag which is by dissolution rather than matte entrainment, as estimated from averaged microprobe analyses of the slags, and overall slag compositions*, %

Operation	Ni	Cu	Co
CSR	71	76	…
NCSR	56	78	50

*The figures express the dissolved metal content as a percentage of the total amount of that metal in slag. Cobalt was not determined for the earlier samples.

not treated by milling and floating. Hence reducing base metal (and associated platinum group elements) losses to slag would require minimisation of dissolution of base metals in the slag, and maximising the settling of entrained matte.

Comparison of the microprobe analysis of the silicate portion of the slag (that is, excluding entrained matte) with the bulk chemical analysis of the tapped slag (including all elements from all phases) allowed estimates of the proportions of the base metals which were lost to the slag in dissolved (oxide) form, rather than as entrained matte. For example, Table 2 shows that, for the CSR operation, the average Ni content (expressed as NiO) of the silicate was 0·16%, whereas the overall Ni content (as NiO) of the slag was 0·19%. The former value is only dissolved nickel, whereas the latter value also includes entrained matte; hence the ratio of the two values gives an estimate of the proportion of nickel which is dissolved. These estimates are given in Table 9, and show that the majority of metal loss is by dissolution. Nickel losses to slag were higher when converter slag was being returned to the furnaces; since losses were mainly by dissolution, the main reason for the greater losses was the more oxidising conditions introduced with the slag feed. The large proportion of losses by solution also explains the observed low recovery of base metals by milling and flotation in the slag plant.

Recycling converter slag to the smelting furnaces is hence contra indicated because it increases the oxygen activity in the slag; this may also increase the danger of magnetite build-up in the furnaces. While the large proportion of oxidic loss suggests a potential advantage of establishing reducing conditions by adding carbon to the feed, this is not currently practical due to the design of the furnace off-gas system.

Loss of entrained sulphide to tapped slag can be controlled by careful tapping practice and level control, and also by blending feed materials to limit slag chromium content. When the chromium content rises above 2%, spinel crystallises and this can impede matte fall, causing matte to be tapped out with the slag.

Conclusion

The combination of electron microbeam techniques with bulk chemistry and Mössbauer spectroscopy has provided important insights into base metal distribution in the furnaces, and the reasons for lower than expected recovery by flotation. Equilibrium calculations of slag losses generally underpredict metal dissolution in the slag if the calculations are based on the composition of bulk matte (rather than entrained matte).

Acknowledgements

The authors would like to thank Anglo Platinum for permission to publish this work, and all the staff at Head Office and Smelters, and at Anglo Research, who have assisted with this project.

References

1. J. Nell: 'Melting of platinum group metal concentrates in South Africa', *J. S. Afr. Inst. Min. Metall.*, 2004, **104**, 423–428.
2. Z. Hofirek and P. Halton: 'Production of high quality electrowon nickel at Rustenburg Base Metals Refiners (Pty.) Ltd', Proc. 20th Annu. Hydrometall. Meet. on 'Electrometallurgical plant practice', Montreal, Canada, October 1990, the Canadian Institute of Metallurgy, 233–251.
3. J. C. Mostert and P. N. Roberts: 'Electric smelting at Rustenburg Platinum Mines Limited of nickel-copper concentrates containing platinum-group metals', *J. S. Afr. Inst. Min. Metall.*, 1973, **73**, 290–299.
4. M. Jacobs: 'Process description and abbreviated history of Anglo Platinum's Waterval Smelter', in 'Southern African pyrometallurgy 2006', (ed. R. T. Jones), 17–28; 2006, Johannesburg, Southern African Institute of Mining and Metallurgy.
5. R. H. Eric: 'Slag properties and design issues pertinent to matte smelting electric furnaces', *J. S. Afr. Inst. Min. Metall.*, 2004, **104**, 499–510.
6. L. Andrews: 'Factors affecting nickel recovery from slags produced during platinum smelting', *Trans. Inst. Min. Metall. C*, 2005, **114C**, 130–134.
7. L. Andrews: 'Base metal losses to furnace slag during processing of platinum-bearing concentrates', MSc dissertation, University of Pretoria, Pretoria, 2008, available at http://upetd.up.ac.za/thesis/available/etd-01222009-172643/
8. R. Fandrich, Y. Gu, D. Burrows and K. Moeller: 'Modern SEM-based mineral liberation analysis', *Int. J. Miner. Process.*, 2007, **84**, 310–320.
9. C. W. Bale, P. Chartrand, S. A. Degterov, G. Eriksson, K. Hack, R. B. Mahfoud, J. Melançon, A. D. Pelton and S. Petersen: 'FactSage thermochemical software and databases', *Calphad*, 2002, **26**, 189–228.
10. L. Andrews, P. C. Pistorius and F. B. Waanders: 'Electron beam and Mössbauer techniques combined to optimise base metal partitioning in the furnace', *Microchim. Acta*, 2008, **161**, 445–450.
11. A. D. Pelton, G. Eriksson and A. Romero-Serrano: 'Calculation of sulfide capacity of multicomponent slags', *Metallu. Trans. B*, 1993, **24B**, 817–825.
12. Y.-B. Kang and A. D. Pelton: 'Thermodynamic model and database for sulfides dissolved in molten oxide slags', *Metall. Mater. Trans. B*, 2009, **40B**, 979–994.
13. E. E. Underwood: 'Quantitative stereology', 109–147; 1970, Reading, MA, Addison-Wesley.
14. S. A. Saltykov: 'The determination of the size distribution of particles in an opaque material from a measurement of the size distribution of their sections,' Proc. 2nd Int. Cong. on Stereology', (ed. H. Elias), 163–173; 1967, New York, Springer.
15. R. C. Urquhart, M. S. Rennie and C. C. Rabey: 'The smelting of copper-nickel concentrates in an electric furnace', in 'Proceedings of extractive metallurgy of copper', vol. 1, 'Pyrometallurgy and Electrolytic Refining', (ed. J. C. Yannopoulos and J. C. Agarwal), 275–295; 1976, Warrendale, PA, The Metallurgical Society of AIME.
16. J. M. Toguri and S. W. Ip: 'Surface and interfacial tension studies in the matte/slag systems', in 'High temperature materials chemistry', (ed. B. C. H. Steele), 199–223; 1993, London, The Institute of Materials.